Video Article

Precise Cellular Ablation Approach for Modeling Acute Kidney Injury in Developing Zebrafish

Rohan Datta[1], Ada Wong[1], Troy Camarata[2], Farhana Tamanna[1], Imran Ilahi[1], Aleksandr Vasilyev[1]

[1]Department of Biomedical Sciences, NYITCOM

[2]Department of Basic Sciences, NYITCOM-A-State

Correspondence to: Aleksandr Vasilyev at avasilye@nyit.edu

URL: https://www.jove.com/video/55606
DOI: doi:10.3791/55606

Keywords: Developmental Biology, Issue 124, Kidney, zebrafish, GFP, epithelial cell, laser, photoablation, confocal

Date Published: 6/3/2017

Citation: Datta, R., Wong, A., Camarata, T., Tamanna, F., Ilahi, I., Vasilyev, A. Precise Cellular Ablation Approach for Modeling Acute Kidney Injury in Developing Zebrafish. *J. Vis. Exp.* (124), e55606, doi:10.3791/55606 (2017).

Abstract

Acute Kidney Injury (AKI) is a common medical condition with a high mortality rate. With the repair abilities of the kidney, it is possible to restore adequate kidney function after supportive treatment. However, a better understanding of how nephron cell death and repair occur on the cellular level is required to minimize cell death and to enhance the regenerative process. The zebrafish pronephros is a good model system to accomplish this goal because it contains anatomical segments that are similar to the mammalian nephron. Previously, the most common model used to study kidney injury in fish was the pharmacological gentamicin model. However, this model does not allow for precise spatiotemporal control of injury, and hence it is difficult to study cellular and molecular processes involved in kidney repair. To overcome this limitation, this work presents a method through which, in contrast to the gentamicin approach, a specific Green Fuorescent Protein (GFP)-expressing nephron segment can be photoablated using a violet laser light (405 nm). This novel model of AKI provides many advantages that other methods of epithelial injury lack. Its main advantages are the ability to "dial" the level of injury and the precise spatiotemporal control in the robust *in vivo* animal model. This new method has the potential to significantly advance the level of understanding of kidney injury and repair mechanisms.

Video Link

The video component of this article can be found at https://www.jove.com/video/55606/

Introduction

Acute Kidney Injury (AKI)[1,2], which also can be referred to as acute renal failure, is broadly defined as a sudden impairment in kidney function[3]. While the level of understanding of this condition has been enhanced remarkably over the years, morbidity and mortality rates have remained high[1,2]. The current treatment for this condition is mostly supportive, as results from multiple clinical trials of drug therapy have been negative[4,5]. The kidney is unique in that it has the ability to repair itself. Therefore, supportive therapy after an early diagnosis of AKI is the best way to limit morbidity[6]. However, it is difficult to detect AKI early, and the mortality rate is a staggering 50-80% for those who require dialysis[5]. With the ability of the kidneys to repair themselves and the lack of treatment options for this condition, it is important to develop methods to enhance this nephron regeneration process.

There have been many different models used for AKI research that includes different agents of injury and animal models. In terms of agents of kidney damage, the aminoglycoside antibiotic gentamicin has been used as a nephrotoxic agent that leads to AKI[7,8]. However, several groups have found that gentamicin treatment is lethal to the zebrafish embryo[9]. It causes tubular damage that is too serious for embryo recovery, making the study of regeneration difficult without some type of intervention. Mammalian models, like the mouse and rat, are also considered valuable, but they face many limitations during the study of AKI. Perhaps the main disadvantage of rodent models is the difficulty in visualizing the rodent kidney and thus determining the precise spatiotemporal processes leading to epithelial death and repair.

Johnson *et al.* have reported a laser ablation-based technique to induce acute kidney injury in embryonic and larval zebrafish[9]. They used pulsed laser ablation to damage the kidney after an intramuscular injection with dextran conjugates. The fluorescence from dextran conjugates allows for the visualization of damage and regeneration in the tubule epithelium[9]. This model overcomes the two limitations mentioned above, but it does not allow for graded levels of injury and is difficult to carry out on large, arbitrary cell groups.

The new laser ablation-based zebrafish model of AKI described here addresses all of the above limitations. The pronephric kidney in larval zebrafish is a mature, functioning organ that contains segments similar to the mammalian nephron, including a glomerulus, proximal and distal tubules, and a collecting duct[10]. Zebrafish larvae are also optically transparent, making it feasible to observe the kidney through fluorescence techniques. Thus, zebrafish are a valuable *in vivo* model of AKI, and the larval pronephric kidney (5-12 days-post-fertilization (dpf)) can be used to study the cellular and molecular processes involved in kidney injury and repair.

This paper presents a method through which specific Green Fluorescent Protein (GFP)-expressing nephron segments can be photoablated using a low-energy (compared to a pulsed-laser system) violet laser light (405 nm). The GFP fluorescence allows for the targeting of a group of

cells, making the changes that occur visible through the observation of GFP photobleaching. In addition, GFP (by absorbing violet light) serves as an energy sink to potentiate the injury in GFP-expressing kidney cells. Time-lapse microscopy can then be used to study the repair process. Studies have found cell proliferation, cell migration, and cell metaplasia[11,12,13] to all be potential processes that may play an important role in kidney repair. However, the relative importance of these processes and the details of their interplay have been difficult to uncover due to the limitations of existing models of AKI. Using this novel approach, it was possible to show that cell migration plays a central role in kidney repair after acute injury[14].

Protocol

This study was carried out in accordance with the recommendations in the Guide for the Care and Use of Laboratory Animals of the National Institutes of Health. The protocol was approved by the NYIT College of Osteopathic Medicine Institutional Animal Care and Use Committee (NYITCOM IACUC). All surgery and *in vivo* experimentation was performed under tricaine anesthesia, and all efforts were made to minimize suffering.

1. Obtaining and Maintaining Embryos

1. Obtain embryos by crossing kidney GFP fluorescent zebrafish.
   NOTE: Examples of fluorescently labeled zebrafish transgenic lines are listed in **Table 1**.
2. Keep the embryos at 28.5 °C in E3 solution during the 24 h post-fertilization.
3. After 24 h, replace the medium with an E3 solution that contains 0.003% 1-phenyl-2-thiourea (PTU).
   NOTE: PTU is used because it blocks the tyrosinase-dependent steps in melanogenesis and hence prevents pigmentation. Here, this solution is referred to as E3-PTU.
4. Raise the fertilized embryos at 28.5 °C until they are >6 dpf, at which point the kidneys have matured.
   NOTE: It is best to use larvae in the 7-9 dpf window.
5. Using a fluorescent dissecting microscope at 40X magnification and green fluorescence emission filters, select the larvae with bright kidney GFP fluorescence.

2. Mounting the Zebrafish for Live-imaging

1. **If photoablating the embryos prior to 3 dpf, remove the chorion from any unhatched zebrafish before mounting the zebrafish for imaging.**
   1. Manually dechorinate with forceps (preferred) or use a chemical treatment with a protease mixture.
      NOTE: Dechorination allows for the best imaging results.
2. Rinse out the chorion debris in the petri dish using E3-PTU solution and refill the dish with E3-PTU.
3. **Prepare 1-2% Low-Melting Point (LMP) agarose with 0.2 mg/mL tricaine solution to mount the zebrafish for kidney photoablation and live imaging.**
   1. If LMP agarose was already prepared beforehand, reheat it in the microwave to melt it.
4. Once the LMP agarose is prepared, place a 35 mm plastic petri dish on a dissecting microscope. Place a pulled glass probe nearby to properly orient the anesthetized larvae.
   NOTE: It is important to do this step in a timely fashion and to have everything in place, because the embryos must be oriented before the agarose solidifies in about 1-3 min.
5. Before transferring the embryo to the agarose, make sure that the agarose is cool (*i.e.* at about body temperature). Use a plastic or glass transfer pipette to place the embryo into the cooled-down melted agarose-tricaine solution.
   NOTE: This is done because agarose that is too hot can be detrimental to the embryo, leading to cardiac arrest or death
6. Using a transfer pipette, redraw the embryo in the agarose solution and position the embryo/larva in the middle of a 35 mm dish.
7. Quickly spread the agarose containing the embryo/larva to evenly cover the bottom of the 35 mm dish; the best volume of agarose to use is ~1-1.1 mL.
8. **Use the glass probe to orient the embryo in the best possible position for photoablation and imaging.**
   NOTE: Movie 1 shows the best orientation of the embryo/larva for unilateral photoablation. This step is the most time-sensitive and should be performed quickly before the agarose starts to gel, as any attempt to reorient the fish after gelling begins is detrimental.
   1. Orient the larva so that the kidney segment of interest is perpendicular to the beam path while the contralateral segment is away from the laser beam (see **Movie 1**).
      NOTE: This can be achieved by turning the larva as shown in **Movie 1**.
9. Allow about 15 min for the agarose to solidify. Cover the petri dish to minimize evaporation. Once the agarose has solidified, the embryo or larva is ready for photoablation.

3. Laser Ablation

1. Operate the confocal imaging system.
   NOTE: When using the referenced imaging platform (see the table of materials), the recommended settings include 40X magnification, a 0.8 NA water dipping lens, and the first dichroic mirror set to allow both 488 & 405 nm illumination of the sample. The detection should be performed on the green channel.
2. Position the dish containing the immobilized zebrafish on a confocal stage.
   NOTE: This procedure is optimized for the upright configuration using a 40-60X water dipping lens. However, it should be possible to modify the procedure for an inverted microscope.

3. In the upright configuration, position the petri dish containing the embryo on top of a microscope slide and keep it in place using modeling clay (*e.g.,* plasticine). Position the glass slide with the petri dish onto the stage of the confocal microscope.
4. Add 3 mL of the imaging solution E3-PTU (see step 1.3) with 0.2 mg/mL tricaine.
   NOTE: The imaging solution can also be added immediately before placing the slide on the stage. The addition of imaging solution should be done very carefully to prevent the agarose from floating off the bottom of the dish.
5. Switch to the water dipping lens (40 or 60X). Slowly raise the stage, making sure that the lens is slightly angled to prevent air from becoming trapped in the beam path. Once the lens touches the solution at an angle, center it so that it is in the field of view of the embryos.
6. Find the segment of interest using the fluorescence light source. Superficially position the branch targeted for injury to minimize light scattering (see **Movie 1**).
   NOTE: The subsequent steps make use of referenced software (see the Table of Materials), but the procedure can be easily adapted to other platforms.
7. Open the software. Navigate to "View"| "Acquisition Control"| "C2plus Compact GUI" and set "pixel dwell time" to "1.9 µs," "frame size" to "512 x 512 pixels," and "pinhole size" to "90 µm." Set "405 nm (or 408 nm in some systems) laser intensity" to zero and "488 laser intensity" to "low" (preferably <1%). Adjust the "gain" to obtain a good dynamic range but not to saturate the signal.
   NOTE: These values are not critical and are used for consistency. When a 405 nm laser is used, it will result in increases in GFP fluorescence. To avoid saturation of the signal during photobleaching (step 3.11), the signal gain value should be scaled down on the green channel. The blue channel gain can be left at zero, as it is not used for sampling.
8. **Click "Scan" in the software interface to scan the kidney using a 488 nm laser. Find the segment of interest that is perpendicular to the beam path and that is well-visualized, with good GFP fluorescence. Once that region has been identified, draw a region of interest using an elliptical Region-of-Interest (ROI).**
   1. Navigate to "ROI" | "Draw Elliptic ROI."
      NOTE: This will be used to continuously measure average GFP intensity while the photobleaching takes place, permitting the administration of a precise dose of laser treatment.

9. Navigate to "View" | "Acquisition controls"| "C2plus Scan Area" and choose "Band Scan Area." The rectangular mask will appear within that interface. Manually define a rectangular scan window using the cursor (*i.e.* drag, resize, and turn the mask) to cover the segment targeted for laser ablation. Right-click within the mask area to accept the selection.
   NOTE: Only the selected region will be scanned.
10. Begin the time measurement while monitoring the green channel using just the 488 nm laser to activate GFP. Ensure that the intensity of the 488 laser is relatively low (~1%). Measure the average intensity of the GFP in the region of interest by selecting "Measure" | "Time Measurement." Use the "Graph" or "Data" tabs to monitor the average intensity values within the ROI.
    NOTE: The rate of acquisition is defined by pixel dwell time and the size of the rectangular window set in step 3.9, but in general, it allows for the fast monitoring of the signal (~2-10 frames/s).
11. **Induce damage to the kidney cells with the violet laser (405 nm) by increasing the intensity to 100% by sliding the "laser power" control all the way to the right. The 488-nm laser can remain active if the intensity is low.**
    1. Observe a line graph using the "Graph" tab or the numerical values of GFP intensity using the "Data" tab and wait until it drops to a desired level, for example 50% of baseline (as shown in **Figure 1**).
       NOTE: A 20 mW laser has been used as part of the referenced laser unit (see the **Table of Materials**); maximal intensity may vary between systems. Lower intensity can be compensated for by longer exposure (*i.e.* using percent GFP bleaching as a measure of total exposure).

12. **Once the GFP intensity within the elliptical ROI (step 3.8) has dropped to a desired level, immediately decrease the intensity of the violet (405 nm) laser to "0" by moving the "laser power" slider all the way to the left in the software control panel.**
    1. Obtain a new baseline of GFP fluorescence. Confirm the ablation by obtaining a ratio of X/Y.
       NOTE: See **Figure 1B**; Y = average intensity before the ablation and X = average intensity after the ablation, using an average of 4 consecutive samples within the ROI. The exact target ratio (50%, 60%, *etc*.) depends on the amount of injury that is desired for a given experiment.

4. Time-lapse Microscopy with Propidium Iodide Staining

1. Apply general time lapse considerations (outlined in a previous study[15]) to visualize propidium iodide staining as a correlate of kidney cell injury after photoablation.
2. Pre-incubate the larvae in 30 µM propidium iodide solution (1% DMSO in E3-PTU) for 3 h prior to embedding and photoablation, as described in steps 2 and 3.7, respectively.
   NOTE: No additional propidium iodide is required in the agarose or the imaging solution.
3. Induce segmental kidney injury, as described in steps 3.1-3.12.
4. Obtain time lapse image stacks, as described in a previous study[14], using a 488 nm laser (GFP) and a 461-nm laser (Propidium Iodide, PI).
   NOTE: The two colors are superimposed in confocal stacks to correlate the disappearance of GFP and the appearance of propidium iodide staining.
5. Set the parameters for obtaining the time-lapse image stacks as follows: virtual slice thickness = 4 µm, z-stack interval = 2 µm, pixel dwell time = 1.9 µs, image dimensions = 512 x 512, and averaging = 2.
   NOTE: These parameters allow for continuous, 10 to 15 min interval recording of up to 4 larvae and ensure that there is minimal photobleaching of the sample.
6. Use imaging software compatible with the recording file format to visualize and analyze the data.

Representative Results

Please note that this protocol was successfully used with a number of kidney GFP transgenic lines, including ET(krt8:EGFP)sqet11-9, ET(krt8:EGFP)sqet33-d10, and Tg(atp1a1a.4:GFP). The example results shown here were obtained using the ET(krt8:EGFP)sqet11-9 line.

Figure 1 shows the example photoablation protocol. The average GFP intensity is monitored inside the region of interest (**Figure 1A**, and **Movie 1**). An example average intensity trace is shown in **Figure 1B**.

As shown in **Figure 2**, after exposure to 405 nm laser light, GFP fluorescence continues to disappear one cell at a time until, at 220 min, the entire ablated segment loses 100% of its GFP positivity. This loss of GFP fluorescence is indeed due to cell death and not, for example, the downregulation of GFP expression. This is evidenced by the appearance of red fluorescent propidium iodide-positive nuclei in the cells that lose GFP positivity.

The extent of cell death can be assessed by measuring average GFP fluorescence in the ablated segment and comparing it to the mean GFP intensity immediately anterior and posterior to the ablated segment. **Figure 3** shows the relationship between the extent of laser exposure (measured by the initial amount of photobleaching) and the extent of cell death in the exposed segment. It shows that, by varying the initial exposure, it is possible to "dial" the injury and the response of the injured epithelium. With 10-20% of initial GFP photobleaching, virtually no reduction of GFP positivity is observed at 5 h post-injury. 50 and 60% photobleaching leads to a complete disappearance of GFP at 5 h, while 30 and 40% bleaching leads to intermediate results, with 50% estimated death observed at about 35% photobleaching. These results are supported by PI staining (**Figure 3B**). 20% photobleaching results in virtually no PI staining at 100 min post-ablation. 50% photobleaching leads to continuous PI positivity in the ablated epithelium after 60 min, while 30 and 40% photobleaching leads to intermediate PI incorporation. As can be seen from this data, this methodology allows for the induction of graded amounts of epithelial injury and for the study of the epithelial response to lethal and sub-lethal epithelial damage.

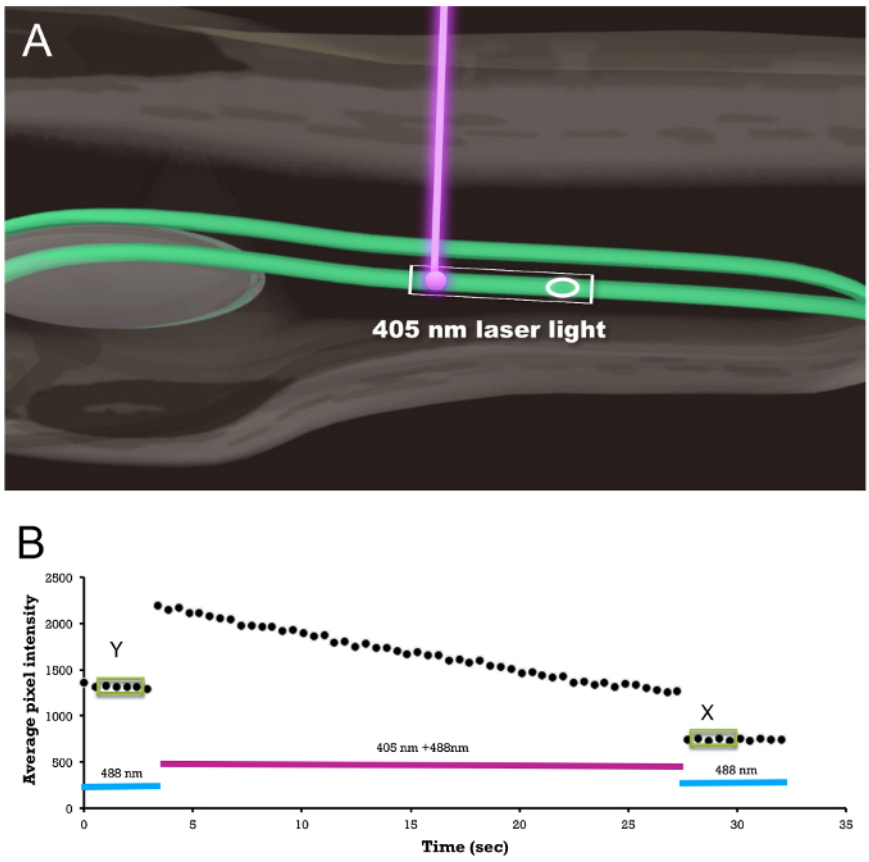

Figure 1: Photoablation Procedure. (**A**) Schematic showing embryo/larva orientation, laser exposure, and the region-of-interest (ellipse) measurement of the average fluorescence to monitor the amount of GFP photobleaching; see Movie 1. The rectangular box indicates the scan window. (**B**) An example of an actual region-of-interest average GFP intensity trace before, during, and after 405 nm laser exposure. Average GFP intensities on four consecutive measurements (shown inside green boxes) are shown before (Y) and after (X) the photoablation. The ratio X/Y is used as a measure of the total light exposure and is plotted on the X axis in **Figure 3**. Please click here to view a larger version of this figure.

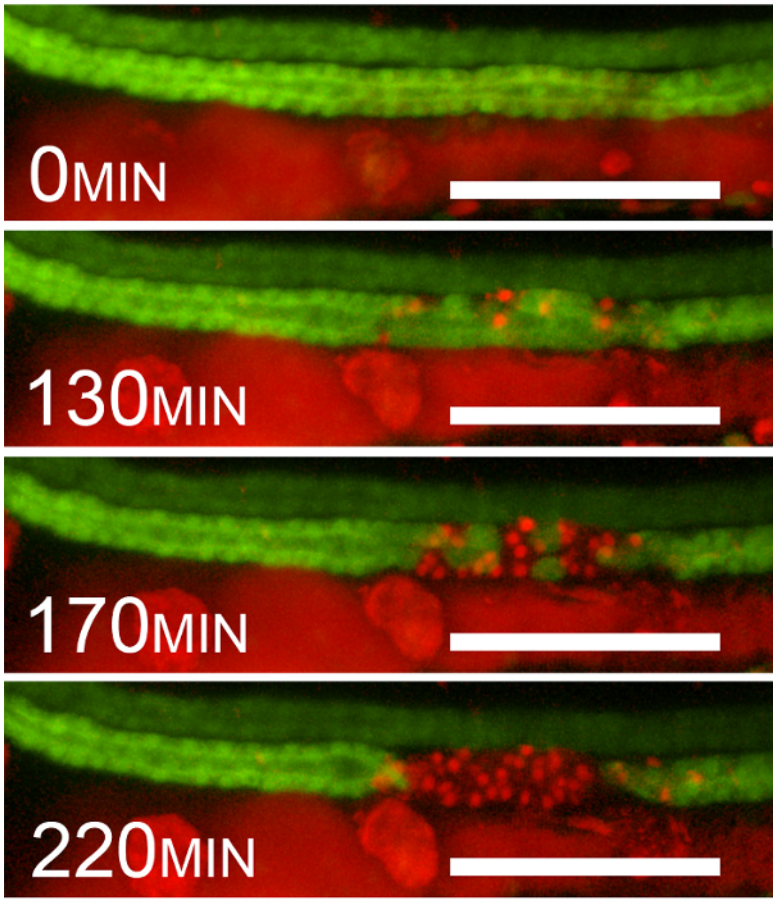

Figure 2: Epithelial Cell Death after 405 nm Laser Exposure. Example sequential frames showing the disappearance of GFP and the appearance of propidium iodide staining after photoablation (40% initial photobleaching). The frames are at 0, 130, 170, and 220 min after violet-light (405 nm) exposure. The disappearance of GFP coincides with the appearance of red fluorescent PI nuclear positivity. Please note that PrI fluorescence is detected by using the red channel. The red fluorescence seen outside the kidney is due to chromophores and the presence of PI in the gut lumen. Scale bar = 100 µm. Please click here to view a larger version of this figure.

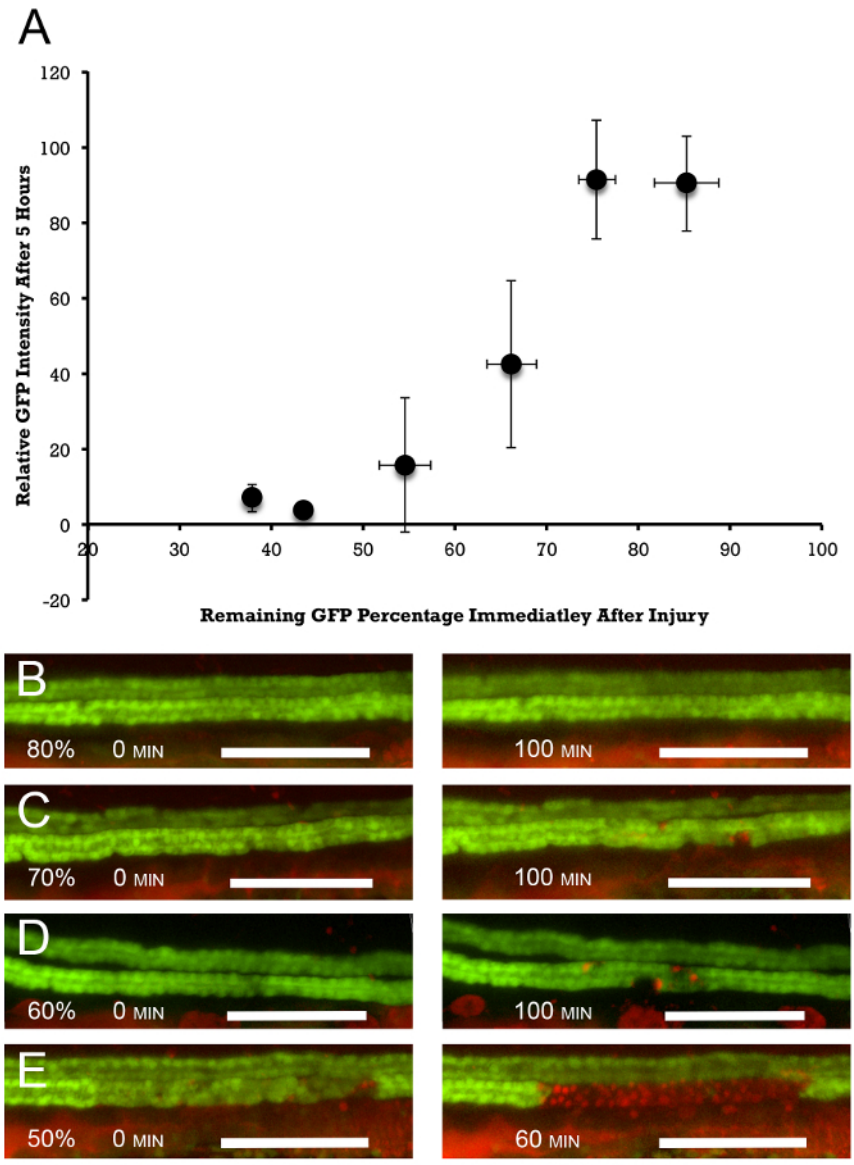

Figure 3: Dose Response of Epithelial Injury to the Amount of Photoablation. (**A**) Photoablation is measured by the percent of initial reduction in GFP fluorescence in the exposed segment. This is compared to the decline in average GFP fluorescence in the injured segment at 5 h post-injury. This measurement is normalized to the average amount of fluorescence upstream and downstream of the injured segment. Target doses were 10, 20, 30, 40, 50, and 60% of the initial photobleaching. The actual amounts are slightly larger, amounting to 14.8, 24.4, 33.8, 45.4, 56.5, and 62.1% photobleaching, which result in 85.2, 75.6, 66.2, 54.6, 43.5, and 37.9% remaining fluorescence, n = 2 - 6/target group. The error bars represent the standard deviation along the X (percent of remaining fluorescence immediately after photoablation) and Y (percent of remaining fluorescence 5 h after photoablation) axes. (**B-E**) PI staining parallels the overall disappearance of GFP positivity. Virtually no PI staining is observed at 20% (80% remaining fluorescence) photobleaching at 100 min post-laser exposure (**B**, right panel). (**C** and **D**) 30 and 40% photobleaching (70 and 60% remaining fluorescence) show increasing numbers of PrI-positive cells (right panels), and (**E**) at 50% photobleaching, virtually 100% PI positivity is observed at 60 min post-injury (right panel). The left panels in (**B-E**) show the initial amount of photobleaching. Scale bar = 100 µm. Please click here to view a larger version of this figure.

Transgenic	Expression Pattern	References
Tg(wt1b:GFP)	Glomerulus, some PT	[11]
Tg(atp1a1a.4:GFP)	Distal to glomerulus	[12]
Tg(cdh17:GFP)	Distal to glomerulus	[9,10]
Tg(ret1:GFP)	Late DT, PD	[13]
Tg(enpep:GFP)	Distal to glomerulus	[14]
Tg(cd41:GFP)	Multiciliated cells	[15]
ET(krt8:EGFP)sqet11-9	Straight PT, early DT	[16,17]
ET(krt8:EGFP)sqet33-d10	Convoluted PT	[16,17]
PT = Proximal Tubule		
DT = Distal Tubule		
PD - Pronephric Duct		

Table 1: Examples of Kidney GFP Zebrafish Lines. Some representative zebrafish lines are listed here, indicating which segment of the pronephric kidney is labeled in a particular transgenic line.

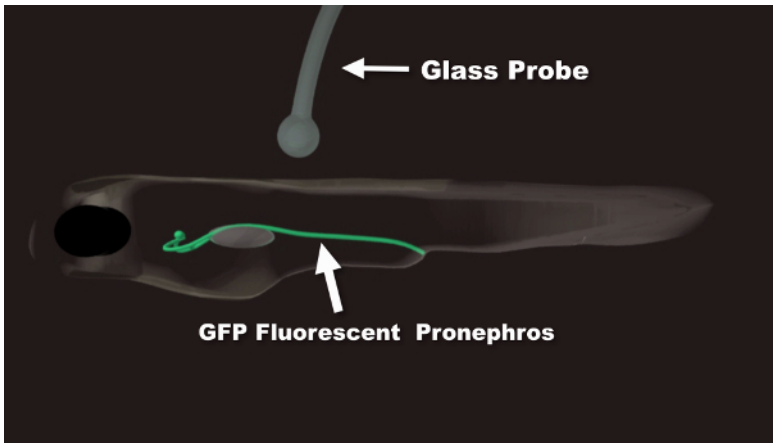

Movie 1: Animation Summary of the Photoablation Procedure. In the first part of the movie, proper embryo/larva orientation is demonstrated. The two kidney branches are shown in green. A glass probe is used to orient the fish in agarose. This is done if a control, non-injured branch is desired. Angling the fish allows for laser exposure on only one branch of the pronephric kidney. In the second part of the movie, the laser ablation procedure is outlined. The ellipse indicates the region of interest within the segment undergoing ablation used to monitor the amount of initial photobleaching. The rectangular window allows for the precise adjustment of the size and position of the ablated segment. Please click here to view this video. (Right-click to download.)

Discussion

It should be noted that the total laser power varies between systems. However, using percent GFP photobleaching allows for a readout of total energy delivered to the fluorescent kidney, independent of the variation in laser power and compensated for by the length of exposure. Keep in mind, however, that the response of different tissues to this method of photoablation varies. Even during kidney maturation, it is significantly more difficult to obtain a 50% reduction in GFP fluorescence in younger embryos than in mature larvae. These differences in tissue responsiveness to photoablation should be taken into account when modifying and adapting this protocol to different applications. Thus, it is critical to monitor the percent reduction in GFP fluorescence to properly gauge the amount of injury and the predicted response of the injured kidney epithelium.

The main advantages of this method when compared other methods of kidney injury in zebrafish is that is allows for the precise control of the spatiotemporal location of the injury. Also, it allows researchers to dial the level of injury up and down. This ability to control the amount of injury should allow for the examination of the responses of epithelial cells and should assist with decision making in terms of recovery versus apoptosis versus necrosis. For example, it is possible to show that cell migration is an initial response of surviving epithelium to segmental ablation and that cell proliferation is a secondary process, likely driven by mechanical forces generated by cell migration[14].

Besides the ability to study the repair process at a cellular level, there are other advantages to this methodology. First, previous photoablation techniques had limited control over the amount of photodamage[9]. However, this model allows for a graded control over the amount of injury, making it easier to conduct future studies. In addition, in this approach, it is possible to target arbitrary groups of GFP fluorescent cells, thus permitting the easy ablation of entire segments. While this could be achieved with the pulsed laser technique, it is more laborious, limiting the potential for experimental design. The use of GFP to target and potentiate epithelial injury is a further advantage, because there are so many GFP transgenic zebrafish available (**Table 1** is only a partial list). Other fluorescent proteins expressed by transgenic species have also been studied, such as the Killer red protein, but these fish transgenics are not widely available[16]. An additional advantage of using GFP is that, with

different laser wavelengths, GFP expression can be used either for photoablation (405 nm) or imaging (488 nm). However, it should be noted that the method published by Johnson *et al.*[9] can be applied to non-fluorescent zebrafish and thus can be used more widely than this approach.

Another limitation of this laser ablation model is that it may not take into account all the different factors that can lead to human AKI. There may be a chain of events that lead to cell necrosis in the human body, as well as cell apoptosis that is induced during kidney injury. It is unclear if the different environment produced during laser ablation can imitate all aspects of the pathophysiology of AKI in humans[10]. Nonetheless, this laser ablation model has many advantages over the alternative models. By allowing for the study of kidney cell death and repair at a high resolution in real time, this method should lead to a better understanding of kidney repair mechanisms and lay a foundation for new approaches to AKI treatment.

Disclosures

The authors declare that they have no competing financial interests.

Acknowledgements

We would like to thank Dr. Iain Drummond and Dr. Vladimir Korzh for sharing kidney GFP transgenic lines. We would also like to thank NYITCOM for providing necessary resources to conduct this work. This study was in part supported by grants: K08DK082782, R03DK097443 (NIH), and the HSCI Pilot Grant (AV).

References

1. Chertow, G. M. "Acute Kidney Injury, Mortality, Length of Stay, And Costs In Hospitalized Patients. *J Am Soc Nephrol* . **16** (11), 3365-3370 (2005).
2. Yasuda, H. *et al.* Incidence And Clinical Outcomes of Acute Kidney Injury Requiring Renal Replacement Therapy In Japan. *Ther Apher Dial* . **14** (6), 541-546 (2010).
3. Waikar, S. S., K. D. Liu, and G. M. Chertow. Diagnosis, Epidemiology And Outcomes of Acute Kidney Injury. *Clin J Am Soc Nephrol* . **3** (3), 844-861 (2008).
4. Lameire, N., Van Biesen, W., & Vanholder, R.. Acute Kidney Injury. *The Lancet.* **372** (9653), 1863-1865 (2008).
5. Esson, M.L. Diagnosis And Treatment of Acute Tubular Necrosis. *Ann Intern Med.* **137** (9), 744 (2002).
6. Vaidya, V.S., Ferguson, M.A., & Bonventre, J.V. Biomarkers of Acute Kidney Injury. *Annu. Rev. Pharmacol. Toxicol.* **48** (1), 463-493 (2008).
7. Hentschel, D. M. Acute Renal Failure In Zebrafish: A Novel System To Study A Complex Disease. *Am J Physiol Renal Physiol* . **288** (5), F923-F929 (2005).
8. Cianciolo Cosentino, C., *et al.* Intravenous Microinjections of Zebrafish Larvae To Study Acute Kidney Injury. *J Vis Exp* (42) (2010).
9. Johnson, C.S., Holzemer, N.F., & Wingert, R.A. Laser Ablation of The Zebrafish Pronephros To Study Renal Epithelial Regeneration. *J Vis Exp.* (54) (2011).
10. Drummond, I.A. and Davidson, A.J. Zebrafish Kidney Development. *Methods Cell Biol.* 233-260 (2010).
11. Toback, F. Gary. Regeneration After Acute Tubular Necrosis. *Kidney Int.* **41** (1) 226-246 (1992).
12. Witzgall, R., *et al.* Localization of Proliferating Cell Nuclear Antigen, Vimentin, C-Fos, And Clusterin In The Postischemic Kidney. Evidence For A Heterogenous Genetic Response Among Nephron Segments, And A Large Pool of Mitotically Active And Dedifferentiated Cells. *J Clin Invest.* **93** (5), 2175-2188 (1994).
13. Bonventre, J. V. Dedifferentiation And Proliferation of Surviving Epithelial Cells In Acute Renal Failure. *J Am Soc Nephrol.* **14** (90001) 55S-61 (2003).
14. Palmyre, A., *et al.* Collective Epithelial Migration Drives Kidney Repair After Acute Injury. *PLoS ONE.* **9** (7) e101304 (2014).
15. Vasilyev, A. and Drummond, I.A. Live Imaging Kidney Development In Zebrafish. *Methods Mol Biol.* 55-70 (2012).
16. Korzh, V., *et al.* Visualizing Compound Transgenic Zebrafish In Development: A Tale of Green Fluorescent Protein And Killerred. *Zebrafish.* **8** (1), 23-29 (2011).
17. Bollig, F., Mehringer, R., Perner, B. *et al.* Identification and comparative expression analysis of a second wt1 gene in zebrafish. *Dev Dyn.* **235** (2), 554-561 (2006).
18. Liu, Y., Pathak, N., Kramer-Zucker, A., Drummond, I.A. Notch signaling controls the differentiation of transporting epithelia and multiciliated cells in the zebrafish pronephros. *Development.* **134** (6), 1111-1122 (2007).
19. Diep, C.Q., Ma, D., Deo, R.C., *et al.* Identification of adult nephron progenitors capable of kidney regeneration in zebrafish. *Nature.* **470** (7332), 95-100 (2011).
20. Zhou, W., Boucher, R.C., Bollig, F., Englert, C., Hildebrandt, F. Characterization of mesonephric development and regeneration using transgenic zebra fish. *Am J Physiol.* **299** (5), F1040-F1047 (2010).
21. Fisher, S., Grice, E.A., Vinton, R.M., Bessling, S.L., McCallion, A.S. Conservation of RET regulatory function from human to zebrafish without sequence similarity. *Science.* **312** (5771), 276-279 (2006).
22. Seiler, C., Pack, M. Transgenic labeling of the zebrafish pronephric duct and tubules using a promoter from the enpep gene. *Gene Expr Patterns.* **11** (0),118-121 (2011).
23. Lin, H.F., Traver, D., Zhu, H., *et al.* Analysis of thrombocyte development in CD41-GFP transgenic zebrafish. *Blood.* **106** (12), 3803-3810 (2005).
24. Choo, B.G., Kondrichin, I., Parinov, S., *et al.* Zebrafish transgenic Enhancer TRAP line database (ZETRAP). *BMC Dev Biol.* **6** (1), 5 (2006).
25. Parinov, S., Kondrichin, I., Korzh, V., Emelyanov, A. Tol2 transposon-mediated enhancer trap to identify developmentally regulated zebrafish genes in vivo. *Dev Dyn.* **231** (2), 449-459 (2004).

